Simulation and experimental validation of heat and mass transfer during hot air drying of wheat grain piles using CFD-DEM under constant-variable temperature

Pengxiao Chen*, Jin Chen, Mengke Fan, Xiaowan Wang, Ruobing Lyu, Ye Liu, Wenxue Zhu, Jianzhang Wu

(*School of Food and Strategic Reserves, Henan University of Technology, Zhengzhou 450001, China*)

Abstract: Achieving rapid and uniform drying of wheat grain piles remains a major challenge because of the complex heat and mass transfer processes within the grain bulk. This study employs a hybrid discrete-continuous 3D model of a wheat grain heap to assess the effects of constant and variable temperature drying (46°C, 56°C, 46°C/16%/56°C, and 56°C/16%/46°C) on mass and heat transfer, as well as drying uniformity. Model validation against experimental data confirmed accuracy, with maximum relative errors below 15.6% for temperature and 4.63% for moisture content. For both constant and variable-temperature drying, the grain pile temperature exhibited a two-stage evolution, with a rapid increase during the initial stage followed by gradual temperature homogenization in the later stage as moisture migration became dominant. The early-stage temperature notably influences temperature and moisture uniformity. Results indicate that higher temperatures improve free water removal but slow its conversion to bound water. Prolonged high temperatures lead to epidermis contraction, internal deformation, and cracking. The findings suggest that variable temperature drying enhances overall drying efficiency and quality. These findings provide theoretical support and practical guidance for optimizing hot-air drying strategies and improving the energy efficiency and product quality of wheat grain drying.

Keywords: wheat grain drying, constant and variable temperature drying, hot air drying, mass and heat transfer, drying process optimization

DOI: 10.25165/j.ijabe.20261904.10040

Citation: Chen P X, Chen J, Fan M K, Wang X W, Lyu R, Liu Y, et al. Simulation and experimental validation of heat and mass transfer during hot air drying of wheat grain piles using CFD-DEM under constant-variable temperature. Int J Agric & Biol Eng, 2026; 19(4): 315–327.

1 Introduction

Wheat is a vital food crop, but in recent years, global warming and frequent extreme weather have led to excessive moisture during harvest and storage, causing significant losses. Effective drying is crucial to minimize these losses and ensure safe storage[1,2]. Currently, hot air drying of wheat is usually done using a constant temperature drying process[3]. It has been found that continuous high-temperature drying leads to surface hardening and internal denaturation of starch pastes. In contrast, prolonged low-temperature drying reduces drying efficiency and adversely affects subsequent storage and quality of the product[4-6]. Variable-temperature drying methods are effective in shortening the drying time of raw materials and reducing the energy consumption in the drying process[7,8]. Variable-temperature drying is widely used in agricultural by-products such as rice[9], shiitake mushrooms[10], and corn[8]. For example, Xu et al.[11] evaluated the effects of constant and variable temperature drying on the quality and drying efficiency of rice in different studies. The results showed that variable-temperature drying not only maintained the quality of rice but also significantly improved the drying efficiency by reducing energy consumption. Li et al.[12] utilized an infrared-assisted spray-bed drying method to dry roses, and the results showed that variable-temperature drying could retain water-soluble polysaccharides in rose petals, but the retention of anthocyanins was poor. In contrast, graded cooling drying was more effective in retaining volatile substances.

Although experimental methods provide valuable information on grain drying, accurately characterizing the coupled heat and mass transfer processes inside grain piles remains challenging. Therefore, with the development of computer technology, numerical simulation has become an important tool for investigating the drying mechanism because of its high efficiency and low cost. Many grain drying researchers have studied the CFD-DEM coupling technique, which combines computational fluid dynamics (CFD) and discrete element method (DEM) to simulate the interaction between airflow and particles effectively and provides a new way of thinking to study the temperature and humidity field and airflow distribution inside the grain pile[13,14]. Munck et al.[15] applied the CFD-DEM fouling law to the fluidized bed solids drying model. Zheng et al.[16] modeled wheat seed heap drying based on the CFD-DEM method. The results showed that the non-uniform porosity distribution model can effectively predict the temperature

Received date: 2025-07-20 **Accepted date:** 2026-07-07

Biographies: Jin Chen, MS, research interest: grain ventilation and drying, Email: 1429117322@qq.com; **Mengke Fan**, MS, research interest: grain ventilation and drying, Email: 3439440290@qq.com; **Xiaowan Wang**, MS, research interest: grain ventilation and drying, Email: 1107797295@qq.com; **Ruobing Lyu**, BS, research interest: grain ventilation and drying. Email: 3481242733@qq.com; **Ye Liu**, MS, research interest: grain ventilation and drying, Email: 1176559243@qq.com; **Wenxue Zhu**, Professor, research interest: agricultural product processing engineering, drying technology and equipment, Email: dry40102@163.com; **Jianzhang Wu**, Associate Professor, research interest: grain ventilation and drying, Email: qlsszz@126.com.

***Corresponding author: Pengxiao Chen**, Associate Professor, research interest: grain ventilation and drying. Henan University of Technology, Zhengzhou 450001, China. Tel: +86-18623710796, Email: cpx2020@haut.edu.cn.

and moisture content of wheat seed heap. Chen et al.[17] combined the discrete element method with the continuous medium method to establish a three-dimensional heap model for wheat drying and analyzed the moisture migration, heat change, and airflow dynamics during wheat grain heap drying. To the best of our knowledge, although numerical simulation has proved to be an effective method for studying food drying, studies utilizing it to establish variable temperature drying processes are still limited.

The objectives of this paper are to use the established wheat seed pile drying model to simulate the constant and variable temperature drying processes; to study the internal structure and moisture distribution changes of wheat during the drying process using low-field nuclear magnetic resonance (LF-NMR) and scanning electron microscopy (SEM); and to validate the model as well as to explore the effects of these processes on the mass and heat transfer and drying uniformity, in order to provide a theoretical basis for the optimization of the hot air drying process and the improvement of the energy efficiency of hot air drying.

2 Modeling of constant-variable temperature drying of wheat grain piles

2.1 Physical model

The physical modeling approach is largely informed by previous research[17]. The model comprises three parts: wheat grain pile structure, inter-grain void, and drying chamber. The hot air inlet, hot air outlet, and model boundary during drying are shown in Figure 1. The wheat grain pile formation process was simulated by compaction using Abaqus software, and the thickness of the wheat grain pile was set to 20 mm.

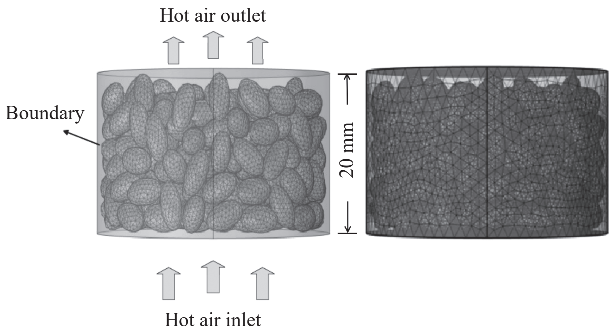

Figure 1 Three-dimensional physical model of wheat grain pile

2.2 Mathematical model

Given that the state of the material in the drying process is very complex, some assumptions must be made to simplify the problem. The specific assumptions are as follows:

1) The particles are assumed to be ellipsoidal on the particle scale, without shrinkage or deformation;

2) The particle pile is assumed to be a discrete solid phase, and the air inside the grain pile is a continuous gas phase;

3) The initial temperature and moisture distribution inside the wheat seeds are uniform;

4) The chemical reactions during the drying of wheat are ignored;

5) The diffusion of moisture inside the grains conforms to Fick’s law, and the fluid flow is considered to be laminar flow.

The model used in this study is as follows[17]:

(1) Momentum equation:

$$\rho\left(\frac{\partial u}{\partial t}+u\cdot\nabla u\right)=-\nabla P+\nabla\cdot(\mu_a(\nabla u+(\nabla u)^{\mathrm{T}}))+F \tag{1}$$

where, ρ represents the density of the fluid, kg/m³; P represents the pressure distribution, Pa; μ_a represents the dynamic viscosity of the fluid, Pa·s; F represents the momentum source term, N.

The initial and boundary conditions are as follows:

$$\begin{cases} t=0,\ \ u=-u_0 n \\ (-\rho I+\kappa)\cdot n=-f_0 n' \end{cases} \tag{2}$$

where, u_0 is the inlet fluid velocity, m/s; κ represents the permeability; f_0 is the normal stress, N.

(2) Energy equation:

Moisture-laden air area:

$$\rho_a C_P u\cdot\nabla T+\nabla\cdot(-k_a\nabla T)=Q+Q_P+Q_{vd} \tag{3}$$

where, k_a is the effective thermal conductivity, W/(m·K); Q is the total energy, W/m³; Q_P is the energy of the porous medium, W/m³; Q_{vd} is the viscous dissipation, W/m³; ρ_a, C_P, and u are the density of hot air, specific heat capacity, and flow rate of the fluid, respectively, in units of kg/m³, J/(kg·K), and m/s.

Porous media area (grain area):

$$C_{P,g}u_a\cdot\nabla T+\rho C_{P,l}u_l\cdot\nabla T+\nabla\cdot(k_{eff}\nabla T)=Q+Q_{evap} \tag{4}$$

where, $C_{P,g}$, $C_{P,l}$ are the specific heat capacity of the mixed gas and water, J/(kg·K); u_a, u_l are the flow rates of the mixed gas and water, m/s; k_{eff} represents the effective thermal conductivity in the grain pile, W/(m·K); Q_{evap} represents the total latent heat source, W/m³.

The initial and boundary conditions are as follows:

$$\begin{cases} t=0,\ \ T=T_0 \\ \text{Inflow:}-nq=\rho_a\Delta H u\cdot n \\ \Delta H=\int_{T_S}^{T}C_P\mathrm{d}T \\ \text{Outflow:}-nq=0 \end{cases} \tag{5}$$

where, ΔH represents enthalpy change; T_0 represents initial stage temperature, °C.

(3) Mass equation:

Moisture-laden air area:

$$\rho_a u\cdot\nabla w_v+\nabla\cdot(-\rho_a D\nabla w_v)=\dot{M} \tag{6}$$

where, w_v represents the mass fraction of water vapor, kg/kg; D represents the effective diffusion coefficient of water vapor, m²/s; $\dot{M}$ represents the mass source term, kg/(m³·s).

Porous media area (grain area):

$$\rho_a u_a\cdot\nabla w_v+\nabla\cdot(-\rho_a D_{eff}\nabla w_v)+u_l\cdot\nabla\rho_l+\nabla\cdot g_{\mathrm{IC}}=\dot{M} \tag{7}$$

$$u_l=-\frac{\kappa_{lr}\kappa}{\mu_l}\nabla P \tag{8}$$

where, D_{eff} represents the effective diffusion coefficient of water, m²/s; u_l represents the fluid flow rate, m/s; g_{IC} represents the evaporation amount of water, kg/(m²·s); κ_{lr} represents the relative permeability of the porous matrix; κ represents the total permeability of the porous matrix, m²; ρ_l represents the density of water, kg/m³; μ_l represents the dynamic viscosity of water, Pa·s.

The initial and boundary conditions are as follows:

$$\begin{cases} t=0,\ \ w=w_0 \\ \text{Inflow:}-n\cdot(-\rho D_a\nabla w_v)=\rho(w_v-w_s)u\cdot n \\ \text{Outflow:}-n\cdot(-\rho D_a\nabla w_v)=0 \end{cases} \tag{9}$$

where, w_0 represents the initial moisture content of the wheat, kg/kg; w_s represents the moisture content of the wheat surface, kg/kg; w_v represents the mass fraction of water vapor, kg/kg; D_a represents the moisture diffusion coefficient in hot air, m²/s.

2.3 Boundary and initial condition settings

The parameter settings are as outlined in Table 1. For variable temperature drying simulations, an If function segment is incorporated, as demonstrated in Equation (10). For constant temperature drying, the variable temperature phase t is set to 0.

$$T(t)=\begin{cases}T_1 & M>M_c\\ T_2=T_1\pm t\cdot v_t & M\leq M_c\end{cases} \quad (10)$$

where, T denotes the inlet air temperature, °C; t represents the time allocated for warming up or cooling down, s; T_1 is the drying temperature during the first stage, °C; T_2 represents the drying temperature during the second stage, °C; M indicates the moisture content of wheat, and M_c is the moisture conversion point, %; v_t is the temperature rise rate in the drying chamber, set at 2°C/min in this study.

Table 1 Material properties of the wheat grain pile model

Parameters	Value or equations	References
Wheat density ρ/kg·m^{-3}	755	Measured
Specific heat capacity of wheat C_p/J·kg^{-1}·K^{-1}	1300+4187M_{db}	Measured
Thermal conductivity of wheat K_{eff}/W·m^{-1}·K^{-1}	0.14+0.68M_{db}	Measured
Effective moisture diffusivity of wheat D_{eff}/m^2·s^{-1}	7.68×10^{-3}exp(–51 080/(8.314 511×(T_a+273.15)))	[18]
Latent heat of vaporization of water h_w/J·kg^{-1}	383.65×(647.1–T)$^{0.316}$	[18]
Effective latent heat of vaporization of wheat h_g/J·kg^{-1}	h_w×(1+23exp(–40M))	[18]
Density of hot air ρ_a/kg·m^{-3}	8.666×10$^{-6}T_a^2$–4.318×10$^{-3}T_a$+1.288	[19]
Specific heat capacity of hot air C_a/J·kg^{-1}·K^{-1}	4.834×10$^{-4}T_a^2$–2.218×10$^{-2}T_a$+1007	[19]
Thermal conductivity of hot air K_a/W·m^{-1}·K^{-1}	–2.401×10$^{-8}T_a^2$+7.554×10$^{-5}T_a$+2.364×10^{-2}	[19]
Hot aerodynamic viscosity μ_a/Pa·s	–3.238×10$^{-11}T_a^2$+4.839×10$^{-8}T_a$+1.73×10^{-5}	[19]
Moisture diffusion coefficient in hot air D_a/m^2·s	3.229×10$^{-10}T_a^2$+1.577×10$^{-7}T_a$+2.089×10^{-5}	[19]

3 Materials and methods

3.1 Experimental materials

Fresh wheat (Zhengmai 126) was purchased from the local farmers' market. The grain sizes were full and undamaged, with an average long-axis diameter of 6.5 mm, a short-axis length of 3.45 mm, thickness of 2.8 mm, and a mass of 0.035±0.005 g per grain. Prior to the experiments, the wheat was refrigerated at 4°C.

3.2 Test methods

3.2.1 Model validation experiment

Uniform distribution of moisture and temperature inside the wheat at the early stage of drying was maintained. A cylindrical drying container (radius 60 mm, height 120 mm) surrounded by wire mesh was used, with wheat initial moisture content of 18 (w.b.), initial surface temperature of 22°C, drying wind temperature of 60°C, and inlet air speed of 1 m/s.

(1) Moisture content verification experiment

The initial moisture content was determined by the oven method before the experiment and repeated three times. During the experiment, the sample mass was taken out and weighed once every ten minutes, the data were recorded and substituted into Formula (10) to calculate the water content (w.b.) at each moment until the moisture content of its wet base reached the safe level (12%±0.5%) when stopping the drying, and the drying experiment was repeated three times.

(2) Temperature verification experiment

In the process of wheat drying, the temperature of the wheat grain pile was measured using a fiber optic temperature sensor. During the measurement process, the light probe was inserted into the top, middle, and bottom layers of the grain pile corresponding to the center and edge areas, and the temperature changes in each internal part were recorded every ten minutes until the end of drying.

After drying for a given time (0 min, 30 min, 60 min), the wheat samples were immediately removed from the hot air drying system and the surface temperature was measured with a thermal imaging camera (testo 875, Testo Instruments International Trading (Shanghai) Co.)

3.2.2 Constant-variable temperature drying experiment

Experiments and simulations were carried out to evaluate the drying of wheat grain piles under various working conditions (constant and variable temperatures), as outlined in Table 2. Wheat with a moisture content of 21.19% was placed into the drying container within the heating chamber of the multiparameter thin-layer drying test bed for hot air drying experiments. They were weighed and recorded every 10 min until the endpoint of drying was reached, and the experiment was repeated three times for consistency. Before the experiment, the wheat was thoroughly mixed. After the equipment was preheated, it was operated under stable conditions, and the same measurement method was used for all data recording.

Table 2 Test program

Test number	Drying method
T_1	56°C constant temperature drying
T_2	46°C constant temperature drying
T_3	46°C/16%/56°C variable temperature drying
T_4	56°C/16%/46°C variable temperature drying

3.2.3 Constant-variable temperature drying simulation experiment

The simulation was configured for four different working conditions as listed in Table 2. It involved solving steady-state laminar flow along with transient heat and mass transfer equations using COMSOL Multiphysics 6.1. This was achieved by selecting the convection-diffusion module and the heat and mass transfer module. The time step was set to 1 minute, with a termination time of 150 min. The simulations were performed on a Dell computer workstation (Win10, Intel(R) Xeon(R) W-2255 CPU 3.70 GHz, 32 G of operating memory), and the computation time was approximately 40 min. The locations of these sampling points are shown in Figure 2.

3.2.4 Low-field nuclear magnetic resonance determination of moisture distribution

Low-field nuclear magnetic resonance (NMR) nondestructive testing, using a variable temperature nuclear magnetic resonance imaging analyzer for food and agriculture, was employed to assess the moisture status during the wheat drying process. Throughout the experiment, 1 g samples of wheat were collected under varying working conditions and at different drying intervals. Each sample was placed in an NMR tube, sealed with cling film, and then positioned within the NMR apparatus for the acquisition of inverse spectra based on the transverse relaxation time T_2.

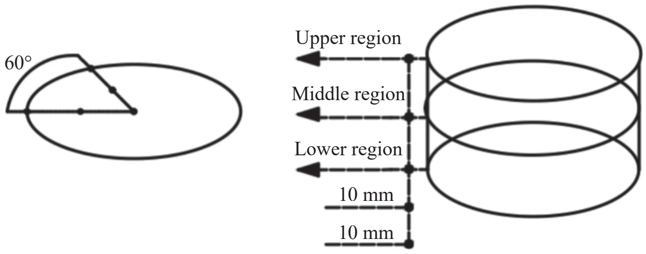

Figure 2 Schematic diagram of simulation test sampling

The parameters for CPMG (Carr-Purcell-Meiboom-Gill) sequence were as follows: main frequency (SF1) at 20 MHz, offset frequency (O1) at 998 629.43 Hz, repetition sampling interval (TW) of 2000 ms, total sampling points (TD) of 140 000, number of echo sequences (NECH) of 7000, echo time (TE) of 0.1 ms, and number of scans (NS) of 64.

3.2.5 Nuclear magnetic resonance imaging experiment

Signal acquisition for moisture distribution during wheat drying was conducted using a nuclear magnetic imaging system. The MRI (Magnetic Resonance Imaging) parameters included: Read size=256 mm, Phase size=128 mm, Averages=32, TR=300 ms, TE=4.41 ms, and Phase encoding duration=0.5 ms.

3.2.6 Determination of microstructure

Full wheat seeds were selected for examination. A scanning electron microscope was used to observe the changes in the sub-microscopic features of the epidermis and seed sections before and after discharge treatment. A knife was used to cut along the middle of the seed ventral groove, and both ends of the wheat seeds were clamped with tweezers to tear the wheat, revealing the inner part. A razor blade was also used to make a parallel cut 2 mm along the wheat ventral groove to obtain epidermal samples. These slices were placed on an electron microscope test bench, glued, coated with gold film using an ion sputtering apparatus, and observed and photographed at different magnifications, such as 300, 500, and 1500 times, to analyze the changes in the microstructure.

3.3 Main evaluation indicators

3.3.1 Method of quantifying moisture content

The specific formulas are provided in Equations (11) and (12):

$$M_w = \frac{m_t - m_d}{m_t} \quad (11)$$

$$M_d = \frac{m_t - m_d}{m_d} \quad (12)$$

where, M_w and M_d denote the wet base moisture content and dry base moisture content of the material, %; m_t denotes the total mass of the sample at time t, g; and m_d denotes the dry matter mass of the sample, g.

3.3.2 Methods for quantifying drying rate

$$\mathrm{DR} = \frac{\mathrm{MR}_t - \mathrm{MR}_{t+\Delta t}}{\Delta t} \quad (13)$$

where, DR denotes the drying rate at moment t, %/min; MR_t denotes the moisture ratio of wheat at moment t, %; $\mathrm{MR}_{t+\Delta t}$ denotes the moisture ratio of wheat at moment $t+\Delta t$, %; Δt denotes the interval between two samples, min.

3.3.3 Method of quantifying the rate of temperature rise

The rate of temperature rise in the wheat grain pile during each drying stage was calculated using the following equation:

$$V_\mathrm{T} = (T_t - T_{t-\Delta t})/\Delta t \quad (14)$$

where, V denotes the rate of temperature rise at moment t, °C/min; T_t denotes the temperature of the wheat at moment t, °C; $T_{t-\Delta t}$ denotes the temperature of wheat at moment $t-\Delta t$, °C; and Δt denotes the interval between two sampling times, in min.

3.3.4 Methods for quantifying drying inhomogeneity

This study analyzes the effects of the drying process on the uniformity of temperature and moisture in the grain pile, using the calculation method developed by Wei et al.[20]. The equation for inhomogeneity calculation is represented by Equation (15):

$$\begin{cases} \mathrm{CV_T} = \dfrac{1}{T_\mathrm{ave}}\sqrt{\dfrac{1}{n}\sum_{i=1}^{n}(T - T_\mathrm{ave})^2} \\ \mathrm{CV_M} = \dfrac{1}{M_\mathrm{ave}}\sqrt{\dfrac{1}{n}\sum_{i=1}^{n}(M - M_\mathrm{ave})^2} \end{cases} \quad (15)$$

where, n is the number of data points; T_ave is the mean value of wheat temperature, K; and M_ave is the mean value of wet basis moisture content of wheat. The CV value (coefficient of variation) is a dimensionless statistic that describes the degree of variation in the data. The smallest $\mathrm{CV_T}$ or $\mathrm{CV_M}$ represents the best heating or drying uniformity.

3.3.5 Total energy consumption

$$E_t = AV\rho_\mathrm{air}C_{p,\mathrm{air}}\Delta T_t \quad (16)$$

where, E_t represents the total energy consumed during the drying process, kW·h; A represents the cross-sectional area of the drying chamber, m^2; V represents the air flow velocity, m/s; ρ_air is the density of air, kg/m^3; $C_{p,\mathrm{air}}$ is the specific heat capacity of air, kJ/kg·°C; ΔT represents the temperature difference between the air inlet and outlet, expressed in degrees Celsius; t represents the drying time, with the unit being hours.

3.3.6 Unit energy consumption

$$SEC = \frac{E_t}{M_\mathrm{evp}} \quad (17)$$

where, SEC is the energy required to dry 1 kg of moisture, kW·h/kg; E_t represents the total energy consumption; M_evp is the mass of evaporated water, kg.

4 Results and discussion

4.1 Model validation

Figure 3 shows the experimental and simulated surface temperatures of a wheat grain pile in a cylindrical vessel subjected to hot air treatment with 60°C hot air. It can be clearly seen that there is a good agreement between the simulated and experimental temperature distributions. In addition, the highest temperatures occur at the edges of the container and the lowest temperatures are located in the center, indicating that the drying is inhomogeneous. Figure 4 shows the temperature change of each monitoring point inside the wheat grain pile. As shown in Figure 4b, the simulated values of wheat kernel temperature during hot air drying were in good agreement with the experimental values, of which the maximum relative errors at the top, the middle, and the bottom are 11.9%, 14.03%, and 15.6% (<20%), respectively. The temperature standard deviation of the three repeated experiments was within ±1.2°C, and the CV range was from 1.2% to 4.5%; the moisture content standard deviation at different time points was within

±0.3% (w.b.), and the CV range was from 0.8% to 3.2%, indicating that the experimental data has good repeatability. The experimental values are always larger than the simulated values, which is because the actual test can not guarantee the adiabatic conditions. The drying container material of the test process is stainless steel; even if the outer wall is wrapped with thermal insulation material, there is a certain amount of heat exchange between the stainless steel outer wall and wheat, which is in line with the viewpoints of Ge et al.[21].

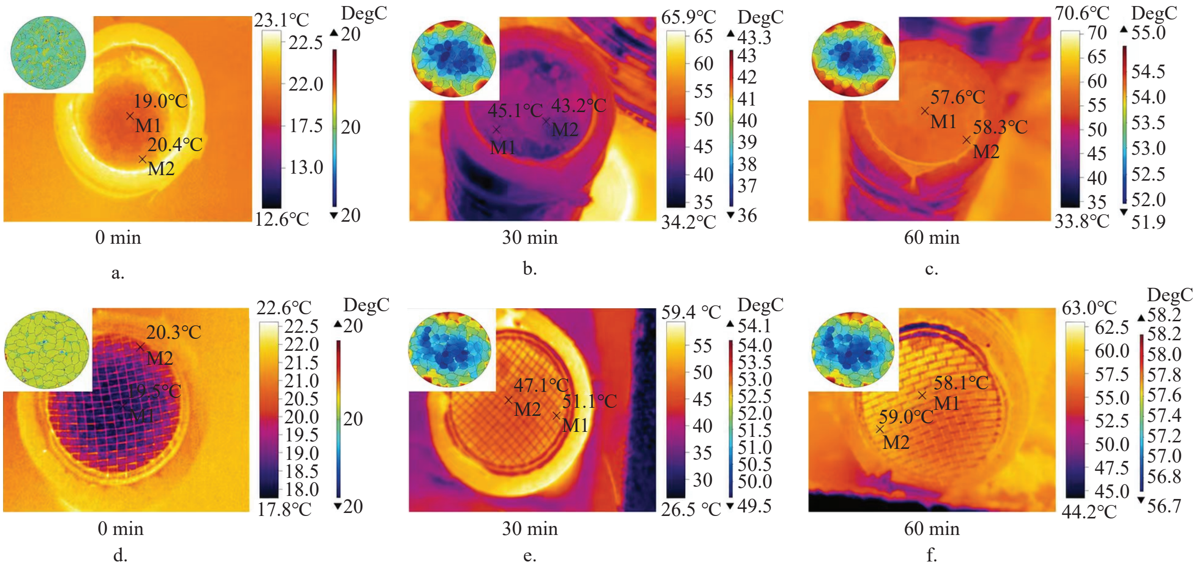

Note: a.-c. 0-60 min upper wheat surface temperature and e.-f. 0-60 min bottom wheat surface temperature.

Figure 3 Surface temperature distribution during drying of top and bottom wheat

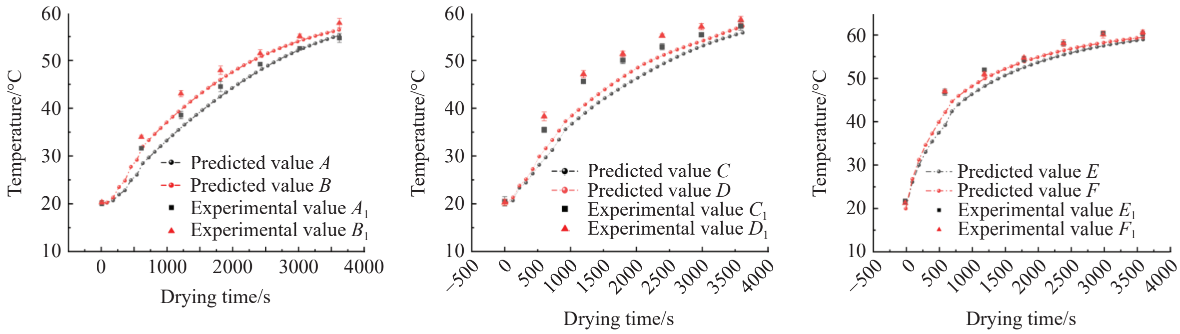

a. Top wheat temperature variation b. Central wheat temperature variation c. Bottom wheat temperature variation

Figure 4 Comparison of simulated and experimental values of temperature at various monitoring points in wheat grain piles

Figure 5 compares the experimental and simulated moisture content-time curves of wheat kernels during hot air drying at 60°C. Figure 5 shows that the experimental and simulated moisture change profiles are highly consistent; the experimental values are marginally higher, with a maximum discrepancy of 4.63%. This is due to the complexity of the water diffusion mechanism in the actual drying process of wheat and the water retention capacity of the wheat grain structure. In conclusion, the model can better reflect the moisture change of the wheat grain pile drying process.

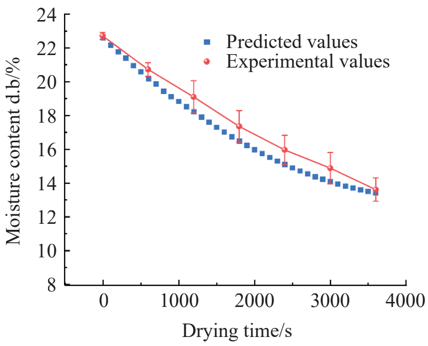

Figure 5 Comparison between simulated and experimental values of wheat moisture content

4.2 The influence of different working conditions on the temperature of the wheat grain pile

Figure 6 shows the temperature distribution of the wheat during a constant temperature drying process (46°C, 56°C) at various moments. As evident from the figure, the temperature distributions for the two conditions (condition T1 and condition T2) have some differences. The temperature at the bottom of the wheat under condition T1 rises to about 50°C by 20 min, with the maximum temperature difference between the top and bottom layers reaching 15°C. This difference gradually decreases within the 20-60 min period compared with condition T1. The maximum temperature difference of the wheat grain pile under condition T2 is 11°C, which is due to the different drying dynamics. The higher the inlet temperature, the higher the temperature gradient between the grain layers, and therefore the larger the temperature difference. At 60 min, the temperature gradient in the grain layers under both conditions was reduced, indicating that the temperature achieved a uniform distribution in the later stage of drying, and the mass transfer process became dominant[22,23].

Figure 7 illustrates the temperature distributions of the wheat during a variable temperature drying process (46°C/16%/56°C, 56°C/16%/46°C) at various times. Unlike the constant temperature setting of 56°C, the overall maximum temperature difference in condition T3 does not exceed 12°C, with the temperature rising uniformly. Condition T4, which involves cooling variable temperature drying, includes both a warming and cooling phase. At 40 min, there are clearly two pre-delay drying fronts. Due to high-temperature ventilation initially, the temperature in the middle area of the wheat is higher than in the upper layer, creating a warm frontal surface. The inlet temperature of 46°C is lower than wheat temperature at the inlet, forming a cold frontal surface during the low-temperature intake in the grain pile. At 60 min and 80 min, conditions T3 and T4 exhibit opposite temperature transfer processes.

Figure 8 displays the temperature change curves of a wheat grain pile under different variable temperature drying process conditions, with the heat transfer rate change curve shown in the lower right corner of the figure. The curves indicate that the temperature change of the grain pile over time can be divided into two stages. In the first 0-5 min, the temperature rises sharply, with a more significant heat transfer rate at higher initial hot air temperatures. From 5 to 10 min, the temperature rise slows down, and by 50 min, the overall temperature of the wheat grain pile approaches that of the hot air. During the drying process, the hot airflow not only facilitates the temperature transfer from the bottom to the top of the grain pile and from the outside to the inside of the seeds, but also accompanies the evaporation of moisture throughout the process. Consequently, part of the heat is consumed for moisture evaporation, resulting in the temperature of the wheat grain pile being generally lower than that of the hot air for most of the drying time[24].

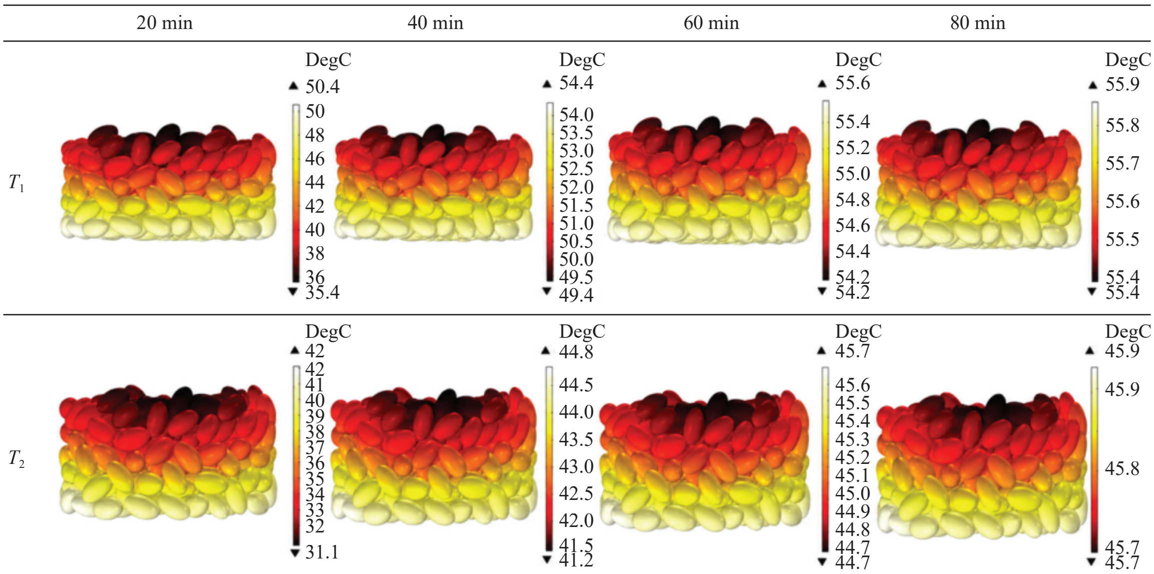

Figure 6 Temperature distribution of wheat in constant temperature drying process

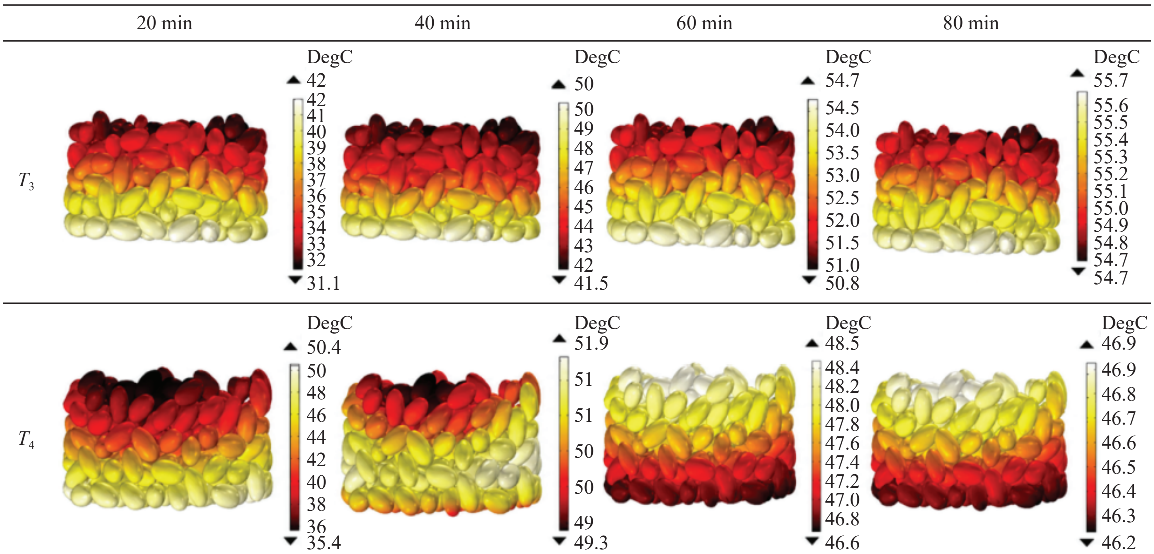

Figure 7 Temperature distribution of wheat in variable temperature drying process

From the curves of working conditions T1 and T2, it is evident that in the initial stage of wheat drying, the hot air temperature significantly influences the rising trend of the average temperature of the wheat grain pile. Within the same ventilation period (5 min), the temperature change rate for condition T1 is 0.0205°C/s, and for condition T2, it is 0.0157°C/s. Observing the curves for conditions T3 and T4, at the node of temperature change, the heat transfer rate for the wheat in condition T3 initially increases from 0.0031°C/s to 0.0096°C/s before gradually decreasing. Similarly, for condition T4, the rate starts from 0.009 61°C/s, drops to 0.007 25°C/s, and then slowly increases. It shows that the higher the hot air temperature, the faster the heat transfer rate of the wheat grain pile.

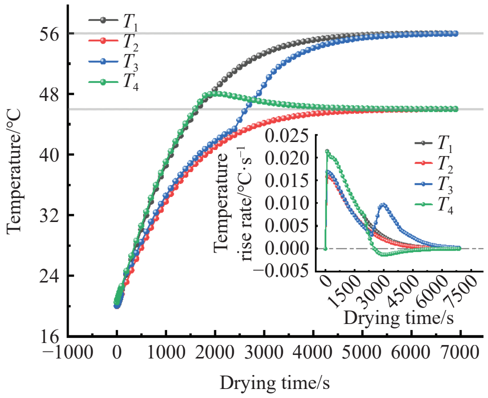

Figure 8 Temperature change rule of wheat drying process

4.3 Effect of different working conditions on the moisture of wheat grain pile

Figure 9 shows the moisture distribution of wheat at various times during constant temperature drying (46°C, 56°C). For single kernels, the high-moisture region converges toward the center, while the low-moisture region expands, enhancing the moisture gradient within the kernel[25]. During drying, hot air enters from the bottom, rapidly evaporating moisture from the lower wheat surface and carrying it upward, which increases moisture absorption in the upper region[17]. As shown in Figure 9, the surface moisture content of the upper wheat grain increased significantly under condition T2 compared to condition T1. This is because the lower inlet air temperature promotes the moisture absorption of the grain particles. Specifically, the lower inlet air temperature in condition T2 resulted in the cold air carrying water vapor flowing through the upper low-temperature wheat region to more easily form condensation on the surface of wheat particles, thereby increasing their surface moisture. This process resulted in the moisture gradient between grain layers becoming more pronounced. Condition T1 reached the drying endpoint at 80 min with even moisture distribution, peaking at 15.7%. In contrast, condition T2, though longer, resulted in more uniform moisture distribution at the end of drying.

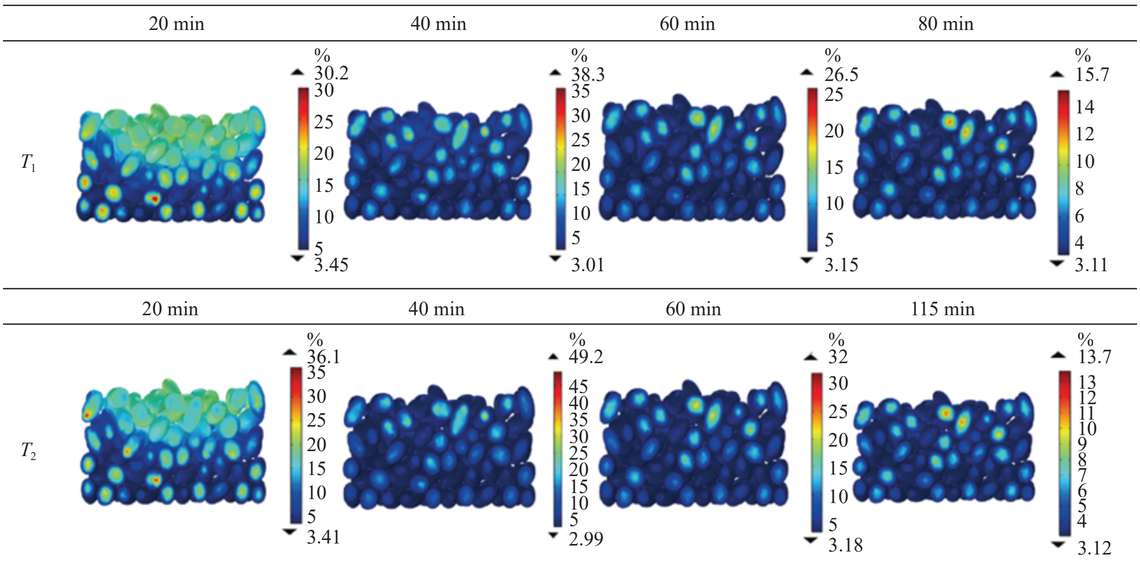

Figure 9 Moisture distribution during constant temperature drying of wheat

Figure 10 displays the moisture distributions of the variable temperature drying process (46°C/16%/56°C, 56°C/16%/46°C) of wheat at different moments. At 40 minutes, under varied temperature conditions, the first stage drying temperature of 46°C established a significant moisture gradient between the wheat grain layers, in contrast to the first stage drying temperature of 56°C. As the inlet temperature increased in the later stages, the moisture gradient in condition T3 diminished. This reduction was attributed to the rise in drying kinetic energy, promoted by the increased temperature, which subsequently lowered the drying resistance in later stages[26].

Figure 11 illustrates the change curve of the wet basis moisture content of a wheat grain pile under different variable temperature drying process conditions. As can be seen from the figure, there is a significant difference in the dewatering process under the four working conditions. The curves demonstrate that the moisture change in the grain pile over time can be divided into three drying phases, primarily the descending drying phase. During the initial 0-5 min, the drying rate of the wheat sharply rises and reaches the maximum value, which is more pronounced at higher initial hot air temperatures. From 5 to 10 min, the moisture drying rate begins to decrease, and by about 50 min, the overall moisture removal rate of the wheat grain heap tends to stabilize at a uniform rate, until the end of drying.

Comparing the drying curves of the four conditions, in the early stage of wheat drying, the hot air temperature significantly influences the overall moisture removal process of the wheat grain pile. Condition T1 and condition T4 have the same rate of moisture change in the first stage, peaking at 0.2513%/min; similarly, condition T2 and condition T3 also have the same rate of moisture change in the first stage, with a peak of 0.2052%/min. Around the temperature change node, 5 min before and after, the drying rate of condition T3 increased by 26.99%, while for condition T4, it decreased by 31.84%. When the constant temperature drying was stepped down from 56°C to 46°C, the entire cooling period lasted 100 min and the drying time extended by 53.33%; conversely, when the drying temperature was stepped up from 46°C to 56°C, the entire heating period required 95 min to reach the new steady-state temperature. This temperature elevation leads to an increase in the water vapor pressure difference between the hot air and the wheat grain heap, accelerating the evaporation rate of the internal moisture of the wheat, and effectively shortening the drying cycle[27].

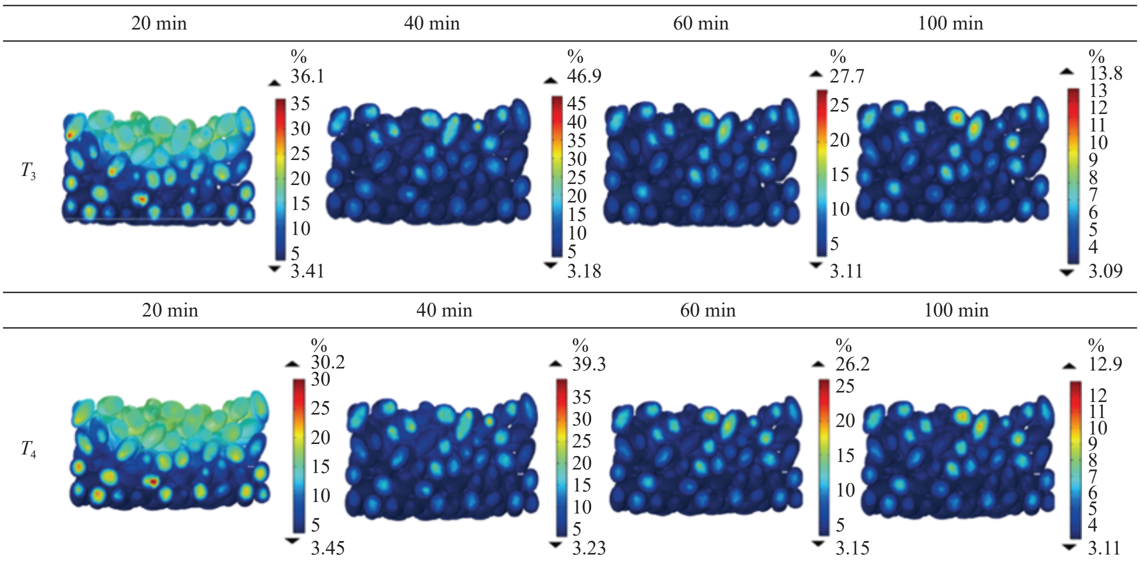

Figure 10 Moisture distribution of wheat in variable temperature drying process

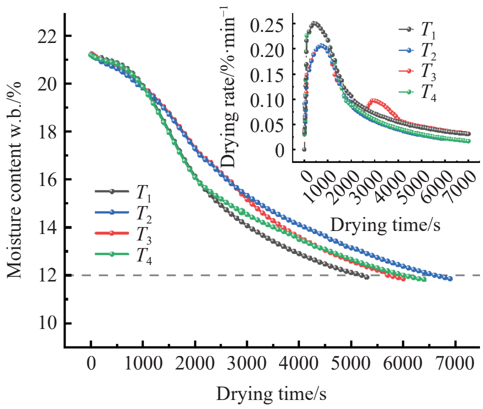

Figure 11 Wheat drying process moisture change rule

4.4 Effect of different working conditions on the unevenness of wheat drying

In the drying process, the temperature inhomogeneity of a wheat grain pile over time is shown in Figure 12. This figure illustrates that the temperature inhomogeneity across different working conditions follows a similar trend: starting with a sharp rise, then gradually leveling off, and finally approaching zero. Conditions T3 and T4, which involve variable temperature drying, exhibit fluctuations in inhomogeneity after the temperature change node. The most significant drying inhomogeneity occurs in the first drying stage, with higher inlet air temperatures correlating with larger CV_T values. Initially, the differences between the layers of the grain pile are minimal. Once the hot air enters the grain pile, it transfers heat to the surface of the wheat through thermal convection. The substantial temperature difference between the high air temperature and the material leads to increased non-uniformity. In the later stages of drying, the primary heat transfer mechanism involves the surface heat being gradually conducted to the cooler parts, reducing the overall temperature difference. Consequently, the impact of the inlet temperature on the temperature of the grain pile diminishes, leading to a decrease in temperature unevenness.

As shown in Figure 12, the initial inlet air temperatures were 46°C and 56°C, with the highest CV_T values recorded at 0.1495 and 0.1863, respectively. In the second drying stage, the temperature under working condition T3 increased, and its temperature inhomogeneity rose from 0.0216 to 0.0428 (an increase of 49.53%). This increase resulted in greater temperature inhomogeneity between the layers compared to working condition T2, which had the same initial temperature. Conversely, in working condition T4, the temperature decreased during the second drying stage, and its temperature inhomogeneity reduced from 0.0439 to 0.0085 (a decrease of 83.9%). This decrease led to lower temperature inhomogeneity between layers than in condition T1, which started with the same initial temperature.

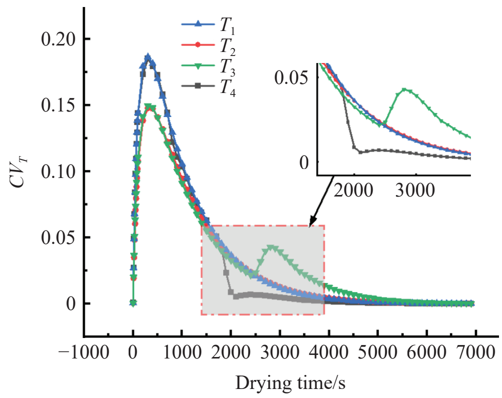

Figure 12 The changing law of temperature inhomogeneity in the drying process of wheat

Figure 13 illustrates the moisture inhomogeneity of wheat grain pile during the drying process, revealing a consistent trend across different working conditions. This trend is characterized by a rapid rise to a peak value followed by a gradual decline. The peak moments of moisture inhomogeneity typically occur when the moisture content is between 17% and 18%, and this inhomogeneity increases with the rise in inlet wind temperature, as reflected by higher CVM values. This increase in inhomogeneity is primarily due to the lower region of the wheat being more directly exposed to the drying medium, resulting in faster moisture removal. Consequently, this accelerates the moisture gradient between the upper and lower layers of the wheat, enhancing inhomogeneity. Moreover, the high porosity of the near-wall region causes the wheat to dry faster than in the center, further amplifying the moisture inhomogeneity across different axial regions of the pile.

In the early stage of drying, the trends of moisture inhomogeneity for wheat across the four working conditions were consistent. The decreasing trend of moisture inhomogeneity slowed down with the temperature increase in the late stage of condition T3, whereas it accelerated with the temperature decrease in the late stage of condition T4, although the overall effect was minimal. This suggests that moisture inhomogeneity is mainly affected by the temperature in the early stage. Specifically, the lower the initial temperature, the lower the CVM, resulting in more uniform drying; conversely, the higher the initial temperature, the higher the CVM, leading to more uneven drying. When the moisture content of wheat is reduced to about 15%, the influence of drying air supply temperature on moisture inhomogeneity of wheat gradually diminishes. This is consistent with the research results of Cheng et al.[28] on the influence of temperature gradient on the moisture migration mechanism during the drying process. The moisture migration rate is mainly affected by internal resistance. In the initial stage, temperature has a significant impact on moisture inhomogeneity. Later, as moisture content decreases and internal equilibrium is established, the influence of temperature gradually weakens.

4.5 Moisture distribution and migration law of wheat drying process under different working conditions

Figure 14 demonstrates the inverse T_2 transverse relaxation time plots for the wheat drying process under four operating conditions. There are three main relaxation peaks in the drying process of wheat: bound water T_{21} (0-1 ms), immobilized water T_{22} (1-10 ms), and free water T_{23} (10-100 ms), with corresponding peak areas M_{21}, M_{22}, and M_{23}, respectively. The test, conducted with rewetted wheat, showed that before drying, T_{22} represented the largest proportion of total moisture, while T_{23} accounted for a smaller proportion, indicating less free water. This is consistent with the findings of Jiang et al.[29]. A significant left shift of T_{22} and T_{23} occurred in the NMR test as the internal structure of wheat crumpled during the middle and late stages of drying, resulting in reduced water mobility and decreased freedom for both immobilized water and free water as drying time progressed[30]. Given the reduced ratio of T_{22} during the drying period, the main source of water dissipation during wheat drying is from the immobilized water.

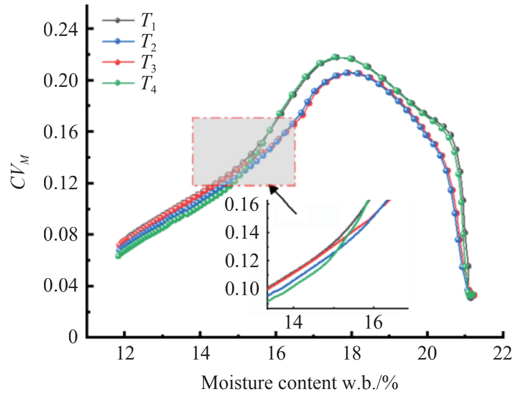

Figure 13 The changing law of moisture inhomogeneity in the drying process of wheat

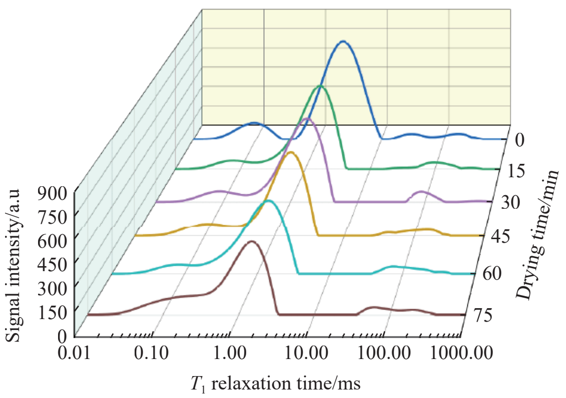

a. Inverse plot of transverse relaxation time for condition T_1

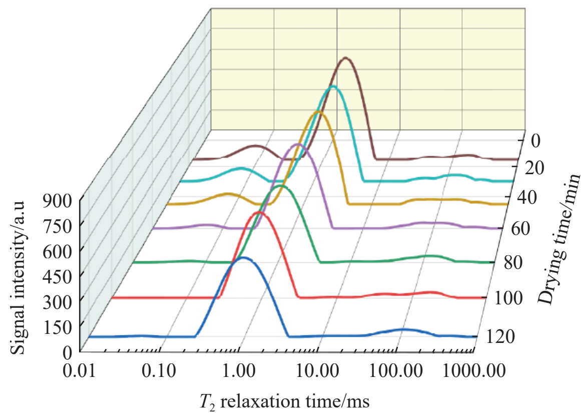

b. Inverse plot of transverse relaxation time for condition T_2

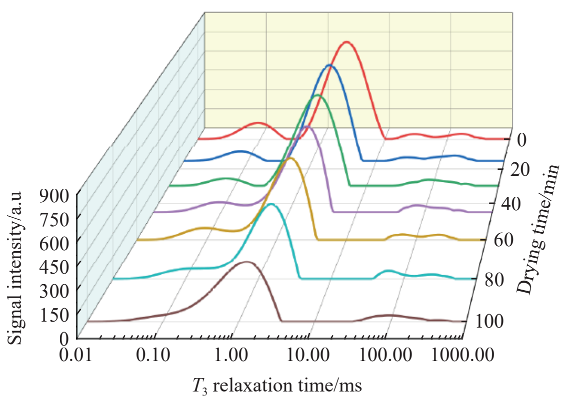

c. Inverse plot of transverse relaxation time for condition T_3

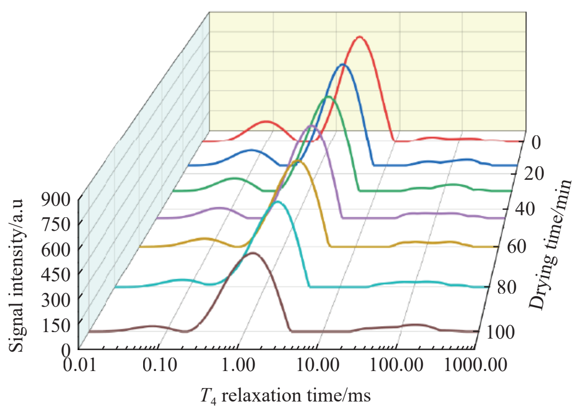

d. Inverse plot of transverse relaxation time for condition T_4

Figure 14 Inverse plot of transverse relaxation time of wheat drying process

As shown in Figure 15, under the four drying conditions, when wheat was dried for 30 min, the amplitude of free water M23 signal was 971.096, 2115.255, 2082.315, 1273.386. This indicates that increasing the first stage drying temperature significantly accelerates the migration and removal of free water. During the first drying stage, the M22 value at a drying temperature of 46°C shows an initial increase followed by a decrease, explained by the gradual aggregation of dispersed free water molecules into more concentrated clusters, transforming free water into a thin layer that tightly envelops the starch granules. At a drying temperature of 56°C, free water is quickly removed without transforming into immobilized water, resulting in a significant decrease in M22. Generally, the peak area of bound water M21 increases under the four conditions, while the peak area of immobilized water M22 decreases the most, likely due to the removal of immobilized water by drying and its transformation into water that is more closely bonded to the material, referred to as bound water. Thus, during the process of wheat drying, there is a noticeable phenomenon of mutual migration and transformation between different states of water.

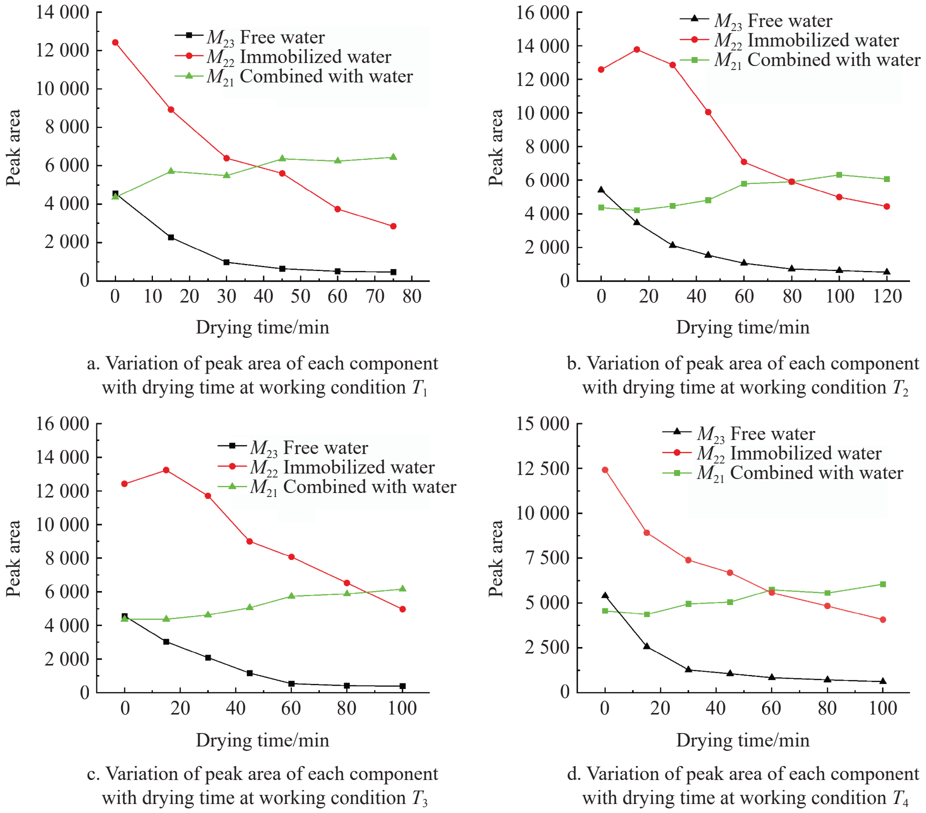

a. Variation of peak area of each component with drying time at working condition T_1

b. Variation of peak area of each component with drying time at working condition T_2

c. Variation of peak area of each component with drying time at working condition T_3

d. Variation of peak area of each component with drying time at working condition T_4

Figure 15 Various relaxation components peak area change curve with drying time

The distribution and migration of water during the wheat drying process are depicted in Figure 16. The figure clearly shows that the proton density map of wheat grains without hot air treatment is more distinct and brighter, with the wheat germ exhibiting higher signal intensity than surrounding areas, indicating higher moisture content in the germ. After drying treatment, the brightness of the proton density imaging diminishes, and the image becomes blurrier, indicating that the moisture of the wheat sample gradually dissipated as drying proceeded. Figure 16 also shows the direction of moisture migration during the drying of wheat kernels, where moisture decreases faster in the epidermal region while consistently showing a stronger signal in the germ. This indicates that moisture always migrates from high- to low-water regions. The germ initially contains more water than the endosperm and, owing to the thermal lag, releases moisture more slowly. When the average kernel moisture reaches the target, the moisture content in the germ is still higher than that in other parts[31].

Comparing the images under different conditions, it was observed that at 15 min, the water signals in the epidermal region for conditions T1 and T4 were weak, while those in the germ region were strong, indicating clear stratification; conversely, for conditions T2 and T3, the water signals inside the wheat kernel displayed a distinct, layer-by-layer decrease. This suggests that higher temperatures in the early stages promote rapid surface water evaporation but may also cause water distribution inhomogeneity within the wheat grain, thereby increasing the moisture gradient between the interior and the surface. Under these conditions, wheat can be subjected to severe mechanical damage due to rapid moisture loss and shrinkage of the outer husk of the kernel. As shown in the figure, 75 min into continuous high-temperature drying (condition T1), the water signals in the wheat grain largely vanished, except in the endosperm, where the hydrogen proton signal remained strong. This indicates that although the high-temperature drying period was relatively short, the moisture distribution at the end of drying was not uniform.

4.6 Effect of different working conditions on the microstructure of wheat

Figure 17 illustrates the changes in the microstructure of the wheat epidermis under different drying conditions: untreated, elevated-temperature drying (46°C/16%/56°C), reduced-temperature drying (56°C/16%/46°C), and constant-temperature hot-air drying (56°C), as shown in Figures 17a-17d, respectively. Figure 17a reveals the smooth surface and reticular structure of the untreated wheat epidermis, characterized by multiple small rectangles. In Figure 17b, after variable-temperature drying with initial warming, the surface of wheat appears smoother, but the rectangular structures are recessed inward, making their outlines more pronounced. Figure 17c, showing the epidermis after cooling and variable-temperature drying, shows a rougher texture and more blurred outlines. Figure 17d demonstrates the epidermis after constant-temperature drying, where the structure appears damaged; the original rectangular outlines are blurred and unrecognizable, accompanied by raised, irregular structures. This damage may be attributed to the contraction and deformation of the internal tissues due to prolonged exposure to high temperatures, leading to the surface hardening phenomenon[32].

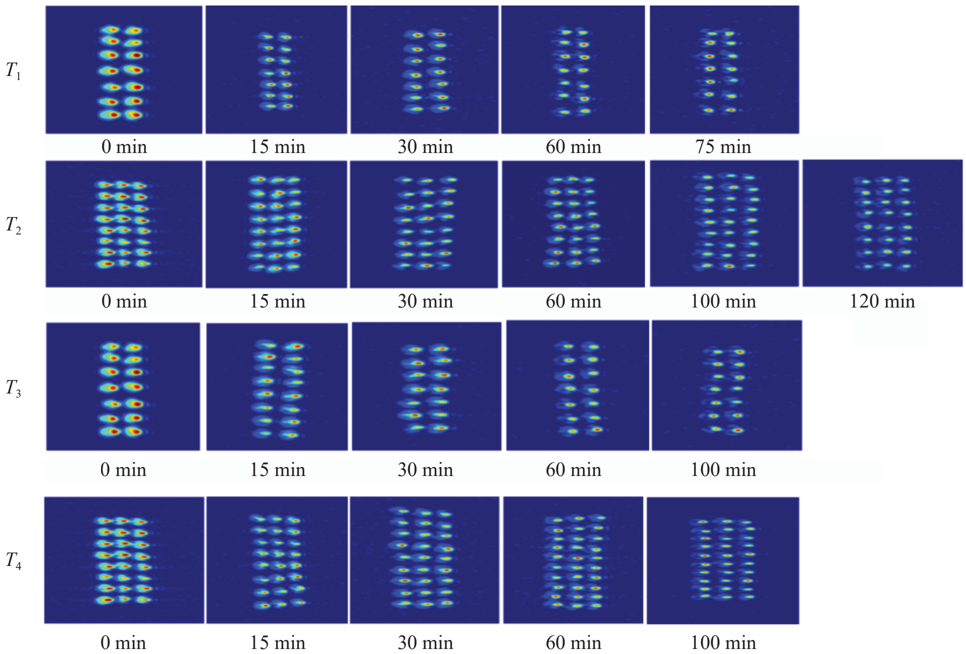

Figure 16 Hydrogen proton imaging during wheat drying at different operating conditions

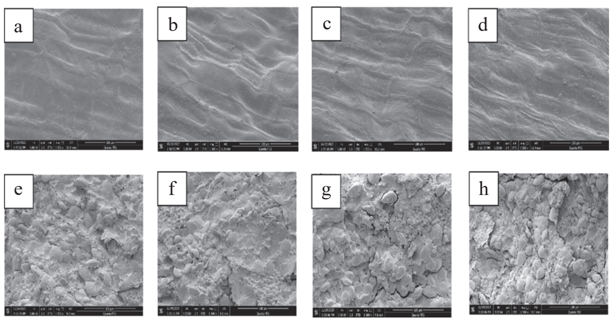

Figure 17 Scanning electron microscopy of wheat epidermis and interior under different drying processes

Figures 17e-17h depict the changes in the internal microstructure of wheat kernels following untreated, elevated-temperature drying, reduced-temperature drying, and constant-temperature drying treatments, respectively. Figure 17e reveals that the internal starch granules of untreated wheat are encased in a protein reticulation structure, showing few cracks and a relatively flat interior. Figure 17f illustrates that after elevated-temperature drying, the free starch granules increase, and the surface becomes rougher. Figure 17g displays the internal structure post cool-down and hot-air drying, where rapid water removal at the early stage of drying leads to an increased number of internal cracks, granular structure, significant structural deformation, and tissue collapse[32]. Figure 17h shows the internal structure of wheat after constant temperature drying treatment, which is like the cooling drying structure, with an increase in the number of internal cracks, deeper cracks, and internal unevenness. This may be due to the change in the stability of starch granules caused by sustained high temperatures, which lead to the phenomena of serious deformation and collapse, and in turn to the deterioration of wheat quality[33]. The results proved that the first stage drying temperature had the most significant effect on the microstructure of wheat. Therefore, elevated variable temperature drying caused the least damage to the epidermal structure of wheat and yielded the best wheat quality.

4.7 Comparison of energy consumption for wheat drying under different working conditions

In constant-temperature drying (46°C and 56°C), the total energy consumption of working condition T1 is 0.12 kW·h, and the unit energy consumption is 1.19 kW·h/kg. The total energy consumption of working condition T2 is 0.08 kW·h, and the unit energy consumption is 0.8 kW·h/kg. The total energy consumption and unit energy consumption of working condition T2 are lower than those of working condition T1. It is indicated that in the process of drying with hot air, increasing the temperature can shorten the drying time and reduce energy consumption[34]. In variable-temperature drying (46°C/16%/56°C, 56°C/16%/46°C), the total energy consumption of working condition T3 is 0.03 kW·h, and the unit energy consumption is 0.38 kW·h/kg. The total energy consumption of working condition T4 is 0.04 kW·h, and the unit energy consumption is 0.41 kW·h/kg. The total energy consumption and unit energy consumption of working condition T3 are less than those of working condition T4. A lower temperature in the initial stage can reduce the internal temperature gradient, avoiding tissue damage caused by local overheating. In the later stage, increasing the temperature can maintain the effective heat transfer force and at the same time make the fluctuation of the drying load more gentle. Variable temperature drying can inhibit surface hardening caused by excessive evaporation in the initial stage, maintain the integrity of the internal pore structure, reduce the resistance to water migration, and provide a continuous channel for water diffusion[35]. Moreover, the total energy consumption and unit energy consumption of variable temperature drying are lower than those of constant temperature drying. Kowalski et al.[36] found through research that compared with drying under static conditions, intermittent drying achieved by variable air temperature and intermittent drying achieved by variable air humidity have lower energy consumption.

5 Conclusions

In this study, a discrete-continuous medium coupling-based variable-temperature drying model for a wheat grain heap was developed and validated through both simulation and experimental analysis of constant-variable-temperature hot-air drying. The following conclusions were drawn:

1) Numerical simulations were conducted to analyze the effects of different drying conditions on temperature and moisture distribution within the wheat heap. The temperature changes in two stages: a rapid rise in the initial phase and uniform distribution in the second phase. Higher hot air temperatures accelerate heat transfer. The two variable-temperature methods (46°C/16%/56°C and 56°C/16%/46°C) showed opposing temperature transfer processes in the second drying stage, with two distinct pre-delay fronts in cooling drying. Moisture changes over time occurred in three stages, with the main phase being descending drying. The shorter high-temperature exposure in the 46°C/16%/56°C process benefits material quality and energy savings.

2) The coefficient of variation (CV) was introduced to quantify moisture distribution uniformity in the wheat heap. Results indicated that the first-stage drying temperature significantly affects uniformity: higher temperatures result in a greater CV for temperature and moisture.

3) During drying, water migrates and transforms, mainly from free to less mobile and then to bound states. The reduction of immobilized water is the primary source of water loss. Higher temperatures accelerate free water evaporation but slow its transformation to an immobile state. Microstructure analysis showed that prolonged high temperatures cause wheat skin shrinkage, internal deformation, and increased cracks.

Acknowledgements

The research was financially supported by the Special Fund for Research on Peanut Heat Pump-Infrared Joint Drying Mechanism and Technology Development, Open Project of Provincial Key Laboratory of Cereal Resource Transformation and Utilization (Grant No. 24400017), Research on Oilseed Soybean RF-Hot Air Joint Drying Technology, Open Project of Key Laboratory of Primary Processing of Agricultural Products at Place of Origin of Agriculture and Rural Development of Ministry of Agriculture and Rural Development of China (Grant No. KLAPPP-2023-02), and Henan Provincial Key Research and Development and Extension Special Project (Science and Technology Tackling) Fund (Grant No. 222102110367).

[References]

[1] Zhu Y D, Shurlknight K L, Chen X X, Sang S M. Identification and pharmacokinetics of novel alkylresorcinol metabolites in human urine, new candidate biomarkers for whole-grain wheat and rye intake. The Journal of Nutrition, 2014; 144(2): 114–122.

[2] Sangha J S, Meyer B, Ruan Y, Cuthbertet R D, Knox R, Xiao G. A pin-based probe for electronic moisture meters to determine moisture content in a single wheat kernel. Plant Methods, 2024; 20: 89.

[3] Cetiner B, Acar O, Kahraman K, Sanal T, Koksel H. An investigation on the effect of heat-moisture treatment on baking quality of wheat by using response surface methodology. Journal of Cereal Science, 2017; 74: 103–111.

[4] Liao Y X, Liu Y X, Zhang W D, Dong H, Yang L Q, Zhang J J, et al. Effects of variable-temperature drying on the qualities and sweet-substance profile of Zizyphus jujuba Mill. cv. Junzao. Food Chem: X, 2024; 22: 101361.

[5] Hossein Nia R, Nalbandi H, Seyedlou S, Salteh S A. Utility of heating pattern with variable air temperature in drying; effects on drying time, energy consumption, and product quality. Food Sci Technol Int. 2023; 31(4). doi: 10.1177/10820132231206435

[6] Deng Z H, Li M, Xing T Y, Zhang J Y, Wang Y F, Zhang Y, et al. A literature research on the drying quality of agricultural products with using solar drying technologies. Solar energy, 2021; 229: 69–83.

[7] Kumar C, Karim M A, Joardder M U H. Intermittent drying of food products: A critical review. Journal of Food Engineering, 2014; 121: 48–57.

[8] Li B, Zeng Z H, Zhang X F, Zhang Y. Study on the variable-temperature drying process of corn drying in an industrial corn-drying system equipped with a self-adaptive control heat exchanger. Applied Sciences, 2021; 11(6): 2772.

[9] Wang H C, Che G, Wan L, Tang H. Effects of drying approaches combined with variable temperature and tempering on the physicochemical quality of rice. Drying Technology, 2023; 41(7): 1199–1213.

[10] Zhang L Z, Jiang L, Xu Z C, Zhang X J, Fan Y B, Adnouni M, et al. Optimization of a variable-temperature heat pump drying process of shiitake mushrooms using response surface methodology. Renewable Energy, 2022; 198: 1267–1278.

[11] Xu X G, Zhao T Y, Ma J N, Song Q, Wei Q, Sun W H. Application of two-stage variable temperature drying in hot air-drying of paddy rice. Foods, 2022; 11(6): 888.

[12] Li L L, Bao Y F, Guo F Z, Chen J L, Zhao M Y, Cao W W, et al. Effect of constant and variable temperature drying processes on drying characteristics, quality, and volatile profile of rose petals in infrared-assisted spouted bed drying. Journal of Food Science, 2024; 89(3): 1387–1402.

[13] Azmir J, Hou Q, Yu A. CFD-DEM simulation of drying of food grains with particle shrinkage. Powder Technology, 2019; 343: 792–802.

[14] Babu A K, Kumaresan G, Aroul Raj V A, Vishal Surya S B. Numerical simulation of heat pump thin layer drying of amaranth leaves. Energy Sources, Part A: Recovery, Utilization, and Environmental Effects, 2023; 45(3): 9383–9395.

[15] de Munck M J A, Peters E A J F, Kuipers J A M. CFD-DEM fluidized bed drying study using a coarse-graining technique. Industrial & Engineering Chemistry Research, 2023; 62(48): 20911–20920.

[16] Zheng D Q, Li L, Chen G X, Zhou Y, Liu K. Numerical study of low-temperature ventilation drying in a wheat grain silo considering non-uniform porosity distribution. Applied Sciences, 2024; 14(1): 96.

[17] Chen P X, Fan M K, Zhu W X, Liu Y, Jiang M M, Wang Y K, et al. Numerical simulation of hot air drying of wheat grain piles based on CFD-DEM and experimental research. Drying Technology, 2024; 42(2): 199–211.

[18] Cao C W, Zhu W X. Computer simulation of agricultural product drying processes. Beijing: China Agriculture Press. 2001. 257p. (in Chinese)

[19] Wei S, Xie W J, Zheng Z H, Yang D Y. Numerical and experimental studies on drying behavior of radio frequency assisted convective drying for thin-layer corn kernels. Computers and Electronics in Agriculture, 2021; 191: 106520.

[20] Wei S, Xie W J, Zheng Z H, Ren L Y, Yang D Y. Numerical study on drying uniformity of bulk corn kernels during radio frequency-assisted hot air drying. Biosystems Engineering, 2023; 227: 117–129.

[21] Ge M M, Chen G X, Liu C S, Zheng D Q, Liu W L. Effect of vertical pressure on temperature field distribution of bulk paddy grain pile. Applied Sciences, 2022; 12(20): 10392.

[22] Wu Z H, Li K, Gao M, Zhao L J, Zhang Z J. Three dimensional body-fitted mathematical model of rice kernel in hot air drying process. Transactions of the CSAM, 2018; 49(1): 329–334. (in Chinese)

[23] Zecchi B, Gerla P. Breakage and mass transfer models during drying of rough rice. Drying Technology, 2007; 25(9): 1405–1410.

[24] Prachayawarakorn S. Drying technologies for foods: fundamentals and applications. Drying Technology, 2019; 37(6): 801.

[25] Jin X, Wang C, Bi Q Y, Liu Z Y, Zhang Z T. Study on drying characteristics of corn based on 3D model. International Journal of Food Engineering, 2020; 16(8). doi:10.1515/ijfe-2019-0320

[26] Li L L, Pan H, Chen J L, Cao W W, Liu W C, Duan X, et al. Infrared-assisted spouted bed drying of Chinese yam cubes: effect of constant and variable temperature drying processes on drying behavior, uniformity, and quality attributes. Journal of the Science of Food and Agriculture, 2023; 103(6): 2815–2823.

[27] Pei Y S, Li Z F, Song C F, Li J, Xu W X, Zhu G Y. Analysis and modelling of temperature and moisture gradient for ginger slices in hot air drying. Journal of Food Engineering, 2022; 323: 111009.

[28] Cheng J H, Zhou X Q, Zhang Y R. Research progress on moisture migration changes and models during grain drying process. Grain and Feed Industry, 2011(7): 13–16. (in Chinese)

[29] Jiang M X, Wu P, Xing H H, Li L, Jia C, Chen S, et al. Water migration and diffusion mechanism in the wheat drying. Drying Technology, 2021; 39(6): 738–751.

[30] Wang X Q, Zhong J H, Han M, Li F, Fan X Y, Liu Y H. Drying characteristics and moisture migration of ultrasound enhanced heat pump drying on carrot. Heat and Mass Transfer, 2023; 59(12): 2255–2266.

[31] Ghosh P K, Jayas D S, Smith E A, Gruwel M L H, White N D G, Zhilkin P A. Mathematical modelling of wheat kernel drying with input from moisture movement studies using magnetic resonance imaging (MRI), part I: model development and comparison with MRI observations. Biosystems Engineering, 2008; 100(3): 389–400.

[32] Hande A R, Swami S B, Thakor N J. Effect of drying methods and packaging materials on quality parameters of stored kokum rind. Int J Agric & Biol Eng, 2014; 7(4): 114–126.

[33] Polat A, Taskin O, Izli N. Intermittent and continuous infrared drying of sweet potatoes. Heat and Mass Transfer, 2022; 58(10): 1709–1721.

[34] Zeng Q Y. Analysis of drying characteristics and energy consumption of sludge at room temperature. Master's dissertation. Guangzhou: South China University of Technology, 2017. (in Chinese)

[35] Zhang L Z, Jiang L, Adnouni M, Li S, Zhang X J. Numerical study on the variable-temperature drying and rehydration of shiitake. Foods, 2024; 13(21): 3356.

[36] Kowalski S J, Pawłowski A. Energy consumption and quality aspect by intermittent drying. Chemical Engineering and Processing: Process Intensification, 2011; 50(4): 384–390.